Biophysical Journal
Article

Biophysical Society

Mechanical limitation of bacterial motility mediated by growing cell chains

Sean G. McMahon,[1] Stephen B. Melville,[2,3,*] and Jing Chen[2,3,*]
[1]Department of Physics, Virginia Polytechnic Institute and State University, Blacksburg, Virginia; [2]Department of Biological Sciences, Virginia Polytechnic Institute and State University, Blacksburg, Virginia; and [3]Fralin Life Sciences Institute, Virginia Polytechnic Institute and State University, Blacksburg, Virginia

ABSTRACT Contrasting most known bacterial motility mechanisms, a bacterial sliding motility discovered in at least two gram-positive bacterial families does not depend on designated motors. Instead, the cells maintain end-to-end connections following cell divisions to form long chains and exploit cell growth and division to push the cells forward. To investigate the dynamics of this motility mechanism, we constructed a mechanical model that depicts the interplay of the forces acting on and between the cells comprising the chain. Due to the exponential growth of individual cells, the tips of the chains can, in principle, accelerate to speeds faster than any known single-cell motility mechanism can achieve. However, analysis of the mechanical model shows that the exponential acceleration comes at the cost of an exponential buildup in mechanical stress in the chain, making overly long chains prone to breakage. Additionally, the mechanical model reveals that the dynamics of the chain expansion hinges on a single non-dimensional parameter. Perturbation analysis of the mechanical model further predicts the critical stress leading to chain breakage and its dependence on the non-dimensional parameter. Finally, we developed a simplistic population-expansion model that uses the predicted breaking behavior to estimate the physical limit of chain-mediated population expansion. Predictions from the models provide critical insights into how this motility depends on key physical properties of the cell and the substrate. Overall, our models present a generically applicable theoretical framework for cell-chain-mediated bacterial sliding motility and provide guidance for future experimental studies on such motility.

SIGNIFICANCE Most known bacterial motility mechanisms rely on designated motors. This work, however, investigates the bacterial sliding motility driven by growing cell chains. This motility mechanism could bring advantages in both performance and efficiency: it can potentially reach very high speeds yet does not require any energy input other than what is already used for cell growth. We modeled the mechanical dynamics of a growing cell chain and revealed a mechanical limit of the chain-mediated motility. The models provide a predictive theoretical framework for future studies of chain-mediated motility, which is likely more widespread among gram-positive bacteria than is currently recognized.

INTRODUCTION

Cell motility allows a cell to adapt better to its environment by moving toward nutrients or away from hazards and allows a cell colony to spread faster and occupy a larger space. In the bacterial kingdom, cell motility is driven by an amazingly diverse spectrum of mechanisms (1–4). The most well-studied mechanism is the bacterial flagellum, a long helical filament that rotates to propel bacterial swimming in liquid mediums (5-7). Another well-studied mechanism is the type IV pilus, which extends from the cell body and attaches to a surface before retracting in order to propel the bacterium on substrates (8–12). Other examined mechanisms include *Mycoplasma* gliding motility, which relies on hundreds of individual motors protruding from the cell surface and exerting power strokes against the substrate surface (13–17), myxobacterial gliding motility driven by motors that exert forces between an internal helical track and the external substrate (18-21), *Spiroplasma* swimming based on propagation of a kink down the helical-shaped cell body (22–24), etc.

All of the bacterial motility mechanisms exemplified above rely on designated molecular motors that consume chemical energy to generate specific modes of mechanical motion and drive single-cell movement. Unlike these mechanisms, many bacteria can exploit the expansive force

Submitted January 5, 2022, and accepted for publication May 12, 2022.
*Correspondence: melville@vt.edu or chenjing@vt.edu
Editor: Alex Mogilner.
https://doi.org/10.1016/j.bpj.2022.05.012

produced by cell growth and division to push on their neighbors, resulting in a "sliding" motility that greatly promotes spreading of the bacterium (25-27). Bacterial sliding has been studied intensively in the context of two-dimensional (2D) biofilm expansion, with popular model organisms such as *Bacillus subtilis* and *Vibrio cholerae*. Growing bacterial biofilms exhibit a number of complex morphological dynamics, including verticalization (28-30), wrinkling (31-33), 2D-to-3D transitions (29,34,35), etc. These dynamics hinge on mechanical interactions among the cells, and many mathematical models have provided valuable insights into how the mechanical dynamics control morphological changes in these biofilms (28,30-41).

Effective sliding motility is typically facilitated by additional cellular factors like secreted surfactants or exopolysaccharides (25). Interestingly, in several gram-positive bacteria, such as *Clostridium perfringens* (42–44), *Clostridium beijerinckii* (44), and *Clostridioides difficile* (11), the sliding motility relies on strong end-to-end connections between daughter cells following cell divisions (42–46). Over multiple cell cycles, long chains consisting of numerous cells form. As the cells in the chain grow and divide, they push each other—this interaction between neighboring cells results in a collective behavior that expands the chain and drives the free tip(s) of the chain forward. Although not requiring any designated energy input other than what is already used for cell growth, the cell-chain-mediated motility can potentially be faster than any single-cell motility mechanism. This is because the number of cells in a chain grows exponentially due to periodic doubling, and consequently, the expansion of the chain as a whole is also expected to accelerate exponentially in time. As a result, the free tips of the chains can, in principle, reach very high speeds. This potentially facilitates the fast penetration of *C. perfringens*, the first bacterium that we know is associated with this cell-chain-mediated motility (42–44), into local zones of patient tissues during the infamous gas gangrene infection it causes (47).

Compared with 2D expansion of biofilms consisting of disconnected cells, cell-chain-mediated sliding provides stronger directionality and is hence more efficient in moving the cells over distances. However, most previous studies on bacterial chains have focused on the morphological changes of the chain over time, using chained *Bacillus subtilis* as a model system (48–53). In this work, we focus on studying how the chain-mediated bacterial sliding performs as a mode of motility, especially in *Clostridia* (42–46).

As the cell-chain-mediated sliding motility hinges on strong cell-cell connections (43,44), the strength of these connection may pose a limit on the motility. To evaluate such a mechanical limit, in this work we developed a physics-based mathematical model to investigate the mechanical dynamics of a growing cell chain. For simplicity, our model focuses on the growth of a single, isolated chain of bacterial cells. The model describes fundamental forces governing the motion of cells in a chain, including the internal growth forces of individual cells, the constraint forces that maintain end-to-end connections between adjacent cells, and the drag forces due to the relative motion between the cells and the substrate. The model shows that the stress between adjacent cells increases exponentially over time and peaks at the center of a chain. Performing a perturbation analysis on the model, we evaluated the mechanical limitation of the chain growth, predicting how long a chain can grow before the stress between adjacent cells builds to an unsustainable level that causes the chain to break. Finally, we developed a simplistic model to evaluate the effect of the mechanical limitation of chain growth on the expansion of the bacterial population. Results from the model inform how the rate of expansion depends on the physical parameters that govern the dynamics of chain growth and provide testable predictions. Of note, our models readily apply to any bacteria that achieve motility based on growing cell chains, whether the motility occurs on solid surfaces or in liquid media. Overall, our models provide a fundamental theoretical framework for investigation of cell-chain-mediated bacterial motility.

MATERIALS AND METHODS

Modeling mechanical dynamics in a growing cell chain

Because growing cell chains rely on clearly defined physical constraints, i.e., the connections between adjacent cells, we can analyze the forces required to push the cells forward in a chain without knowing any details of the molecular mechanism. Hence, we chose to start our investigation with mathematical modeling of the mechanical dynamics of single chains of rod-shaped bacteria. Specifically, we designed the model to investigate the interplay of various forces acting on the bacterial cells forming the chain. The key assumptions of this mathematical model are summarized below and in Fig. 1. A more detailed description of the mathematical model can be found in Section S2 of the supporting material.

- A chain consists of cells that are rigid, inflexible rods (Fig. 1 *A*). Adjacent cells in the chain are mechanically connected at their ends and therefore are physically constrained by one another.
- Each pair of adjacent cells are joined by an angular spring that exerts a torque on the two cells and forces them to align. The angular springs have a potential energy of $E_{b,i} = \frac{1}{2} k_b(\theta_{i+1} - \theta_i)^2$ (Fig. 1 *B*).
- The cell experiences an anisotropic viscous drag force from the substrate. Fig. 1 *C* and *D* shows the decomposition of velocities and drag forces used in this anisotropic implementation (54,55).

To depict the growth dynamics of individual cells, we assumed that the cell length increases exponentially in time (Eq. S1) (56,57), and once the cell length doubles, cell division occurs, and the cell length halves (Fig. 1 *A*, *inset*). Furthermore, we assumed that all cells in the chain operate with synchronized cell cycles, i.e., having the same length at all times and dividing simultaneously. These assumptions capture the exponential acceleration of the cell-chain-mediated motility while greatly simplifying the mathematical analyses to be shown below. The qualitative conclusion of the model does not rely on these convenient assumptions though.

We used the Lagrangian mechanics formalism to derive the differential equations that describe the movement of bacterial cells in an expanding chain (Eqs. S13–S15). Details of the derivation of these equations are

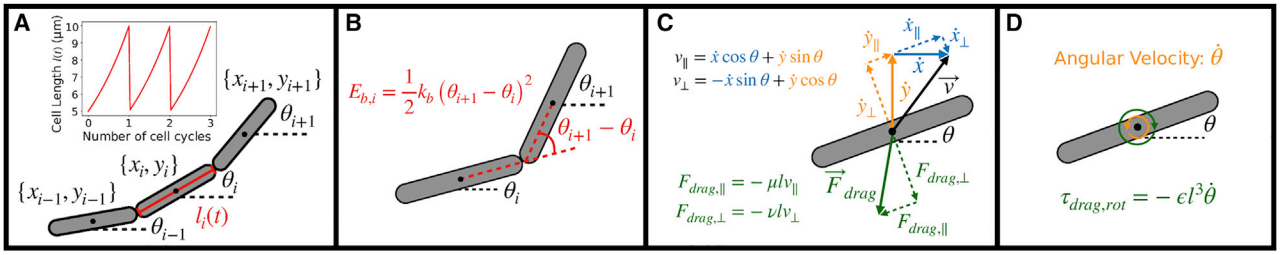

FIGURE 1 Mechanical model for a single growing cell chain. (*A*) Variables in the model. Cells form chains due to strong end-to-end connections between adjacent cells. In the mathematical model, the cells in the chain are uniquely described by their center of mass coordinate, (x_i,y_i), and their angle from the horizontal line, θ_i. The inset provides an example of the temporal change of the length of a single cell over multiple cell cycles. The length of each cell increases exponentially with rate r, $l_i(t) = l_0 e^{rt}$, until the length is double the cell length at the beginning of the cycle, i.e., $2l_0$. At this point, the cell divides into two daughter cells, each with length l_0, and the cycle is repeated. (*B*) Bending between adjacent cells is modeled as an angular spring located at the linkage between the cells. $E_{b,i}$ is the potential energy of the angular spring. The angular spring results in a torque that attempts to push the cells toward alignment. (*C*) Viscous drag from the substrate is decomposed into an anisotropic translational drag force. The velocity of the cell is decomposed into x and y components, which are further decomposed into parallel and perpendicular velocity components. Due to the rod shape of the cell, the parallel translational drag is expected to be smaller than the perpendicular drag (supporting material, Section S2.1). (*D*) A rotational drag torque is exerted on the cell in the direction opposite the angular velocity of the cell's rotation about its center of mass. The relations between the two translational drag coefficients and the rotational drag coefficient are governed by the physics of viscous drags, with the estimation given in the supporting material, Section S2.1. To see this figure in color, go online.

provided in Section S2.2 of the supporting material. Strikingly, nondimensionalizing these differential equations (Eqs. S22–S24) reveals a nondimensional parameter,

$$\Psi = \frac{k_b}{\mu l_0^3 r}, \tag{1}$$

which relates the key physical parameters, including the daughter cell length l_0, the growth rate r, the angular spring constant k_b, and the parallel drag coefficient per unit length μ. In the following sections, we will analyze these differential equations both analytically and numerically in order to quantify the dynamics of the forces governing the expansion of these chains and investigate the mechanical limitation on chain expansion.

RESULTS

Chain-mediated sliding motility is widely observed in gram-positive, rod-shaped bacteria

We first observed cell-chain-mediated sliding motility in the pathogen *C. perfringens* (42–44). Although *C. perfringens* was once believed to be a nonmotile bacterium (58), it can penetrate human muscle tissues by several centimeters per hour and cause acute gas gangrene infections with a nearly 100% mortality rate if not treated (47). It was lately discovered that, when starved, *C. perfringens* cells form long chains through maintaining strong end-to-end connections between daughter cells following cell divisions (42–46). These chains often extend from a colony of *C. perfringens* (cf. Video S3 of (43)) but can also grow from a single isolated cell (Videos S1 and S2). Such cell-chain-mediated motility hinges on a strong connection between neighboring cells (43,44). Although *C. perfringens* possesses type IV pili (11,44,59,60), the pili themselves are not required for its motility. The chain-mediated motility allows fast and often asymmetric expansion of the bacterial colony on the substrate surface (42,43,46). We also found *Clostridium beijerinckii* (44) and *Clostridioides difficile* (11) exhibiting a similar sliding motility driven by the formation of long bacterial chains. Notably, another group of gram-positive bacteria, the bacilli, in particular, *Bacillus subtilis* and *Bacillus megaterium*, also exhibit similar chain-mediated sliding motility under comparable experimental conditions (Fig. S1; Videos S3 and S4). Taken together, it is likely that the cell-chain-mediated sliding motility is widespread among gram-positive, rod-shaped bacteria.

Likely widespread, the dynamics and efficacy of the cell-chain-mediated sliding motility are worth investigating. In this work, we addressed the question with mathematical modeling. While the models we developed are generally applicable to any bacteria utilizing the cell-chain-mediated motility, here we used *C. perfringens* as our experimental model organism, on which all the quantitative experiments were conducted.

Stress in the cell chain is unsustainable due to exponential increase

Applying the rigid-rod model to a perfectly straight chain of cells reveals key behaviors of the stress in the chain over time. Given a perfectly straight chain that starts with N cells, each with length l_0 at the beginning of a cell cycle, the total length of the chain as a function of time is given by $L(t) = Nl_0e^{rt}$. (Because a cell division does not alter the summed length of the two daughter cells, the total length of the chain appears to grow continuously in an exponential manner. The exponential function partly reflects the exponential increase of cell length and partly the exponential increase of cell number.) A given cell-cell linkage divides the chain into two pieces with lengths $l_1(t) = qL(t)$ and $l_2(t) = (1 - q)L(t)$, where q denotes the relative position of the linkage

in the chain (Fig. 2). Since all cells in a perfectly straight chain lie parallel to the x axis, the y components of the stresses must all be zero by symmetry. Solving the equations of motion in our model yields an analytical expression for the stress in the x direction at each cell-cell linkage:

$$F(t,q,N,\mu,r,l_0) = \frac{1}{2}q(1-q)N^2\mu l_0^2 r e^{2rt}. \quad (2)$$

The most revealing information from Eq. 2 is that the stress grows exponentially in time (Fig. 2 *A*). Note that although this exponential increase in the stress is derived from the exponential growth of individual cells, the latter is not essential, as periodic doubling of the number of cells in the chain alone can result in an exponential increase in the stress, regardless of the detailed dynamics in individual cells. It is essentially the exponential increase of the cell number in the chain that causes the exponential increase in the stress. In light of this finding, while the exponential growth of cell number allows a chain to expand exponentially, this fast mode of expansion must be unsustainable, given that the stress in the chain also increases exponentially. Exceedingly high stress in a cell-cell linkage would cause the linkage to fail and the chain to break into shorter chains. The shorter chains will then expand at a slower rate, limiting the speed with which the cells at the tip of the chain can move and the cell population can expand spatially.

Equation 2 also suggests that the stress is largest at the center of the chain and decreases in the joints closer to the free tips of the chain (Fig. 2 *B*). Accordingly, one would expect a chain with two free ends to break most likely in the middle. This was indeed observed in our experiment: 58% of experimentally observed *C. perfringens* chains broke within 10% of the center of the chain (Fig. 2 *C*), with a typical example shown in Video S1.

So far, our model has suggested that a mechanical limit exists for the cell-chain-mediated sliding motility. In the following two sections, we will quantitatively evaluate the limit and determine its effect on the spatial expansion of the bacterial population.

Cell chains break at a critical stress

In this section, we used the rigid-rod model to estimate the critical stress that causes a growing cell chain to break. A cell chain breaks when a cell-cell linkage snaps due to being overly bent, as experimentally observed in *C. perfringens* doublets that happened to be stuck to the substrate at their free ends (Video S5). We first simulated the rigid-rod model to examine the dynamic process leading to a break event. Because a perfectly straight cell chain will never bend in our deterministic model, we initiated the model simulation with a straight chain with a slightly kinked center linkage. In the simulated chain dynamics (Video S6), as the chain elongated and stress built up, the kinked center linkage of the chain started to bend severely after a while. In the model, the cell-cell linkages were perpetually maintained, causing the cells surrounding the center linkage to also tilt. In reality, however, a linkage would snap when bent over a limit (Video S5). After the most stressed center linkage snaps, stress is immediately reduced in the nearby linkages (as they are now close to a free tip), and the tilted parts of the chain will likely be straightened by the angular spring forces. Most importantly, the simulation result (Video S6) displays a transition from a phase in which the chain smoothly grew to a phase in which the angle of the center linkage increased in an accelerating manner. This result reveals a general path to mechanical instability and chain breakage in the system: if the angle of a cell-cell linkage in the chain starts to increase, the system passes a point of no return, followed soon by over-bending and breakage of the linkage.

In light of the finding above, we devised a perturbation analysis for the model to evaluate the critical stress that

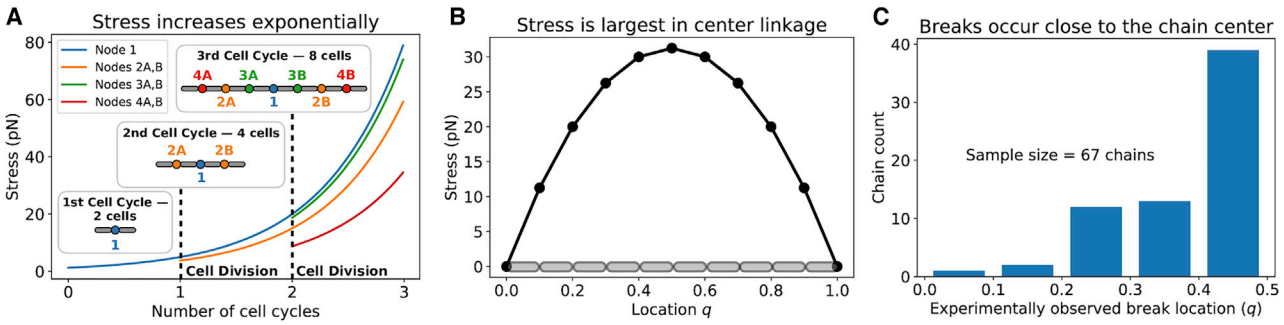

FIGURE 2 Stress in a straight chain increases exponentially and is largest in the center linkage. (*A*) The stress in the linkages of a perfectly straight chain as a function of time over the course of three cell cycles. The chain consists of two cells in the first cell cycle, four cells in the second cell cycle, and eight cells in the third cell cycle. Results were calculated using Eq. 2. (*B*) The stress as a function of location in a perfectly straight chain. The location index, $0 \le q \le 1$, defines the relative position of the linkage in the chain, where $q = 0$ corresponds to the left tip of the chain and $q = 1$ corresponds to the right tip of the chain. Parameter values used in (*A*) and (*B*): $l_0 = 5$ μm, $r = 0.02$ min^{-1}, $k_b = 500$ pN μm, and $\mu = 5$ pN min/μm^2. (*C*) The distribution of break locations in experimentally observed *C. perfringens* chains. The locations are reported using the relative location index q with all values mapped onto the interval between 0 and 0.5, given the symmetric nature of the chains and arbitrary choice of which end corresponds to $q = 0$. To see this figure in color, go online.

causes the angle of a cell-cell linkage to start increasing in a growing cell chain. Particularly, we consider a chain slightly perturbed from the straight geometry: all cells lie parallel to the x axis except for two adjacent cells, which are tilted away from the x axis by a small angle. The linkage between the two tilted cells is called the perturbed linkage, and the size of this perturbation is the angle $\Delta\theta$ between the two tilted cells (Fig. 3 *A*). A perfectly straight chain of cells is considered the "steady state" in the analysis, and the chain with the two tilted cells is the "perturbed state" (Fig. 3 *A*). The perturbed state mimics small perturbations that would occur in reality due to bumps in the substrate, random fluctuations in cell growth, etc. The fate of the perturbed system can be predicted by examining the instantaneous rate of change of the perturbation angle $\Delta\dot{\theta}$ in a perturbed state with a given $\Delta\theta$. If $\Delta\dot{\theta} > 0$, then the size of the perturbation is increasing, and the system is moving away from the perfectly straight steady state (Video S7). This will soon lead to over-bending of the linkage and breakage of the chain. If $\Delta\dot{\theta} < 0$, then the size of the perturbation is decreasing, and the system is moving toward the perfectly straight steady state (Video S8). In this case, the chain "survives" the perturbation. Note that $\Delta\dot{\theta} < 0$ only means that the chain will not immediately over-bend and break; as the chain further grows, the stress will eventually exceed the limit, causing the chain to break. In other words, $\Delta\dot{\theta} = 0$ marks the critical point when a small perturbation can escalate to chain breakage shortly.

Furthermore, to evaluate $\Delta\dot{\theta}$ for linkages under different stresses, we consider the center linkage in chains with different numbers of cells. According to Eq. 2, longer chains with more cells experience higher stress at the center linkage than shorter chains with fewer cells. Computation of the instantaneous $\Delta\dot{\theta}$ using the rigid rod model reveals that $\Delta\dot{\theta}$ increases with the length of the chain and changes sign at the same chain length for different sizes of perturbation, $\Delta\theta$ (Fig. S2). Replotting the computed $\Delta\dot{\theta}$ against the stress in the corresponding cell-cell linkage in the perfectly straight steady state reveals the "critical stress" that differentiates the fate of the perturbed chain (Fig. 3 *B*).

Alternatively, we could vary the stress in the perturbed linkage by imposing the perturbation at different locations

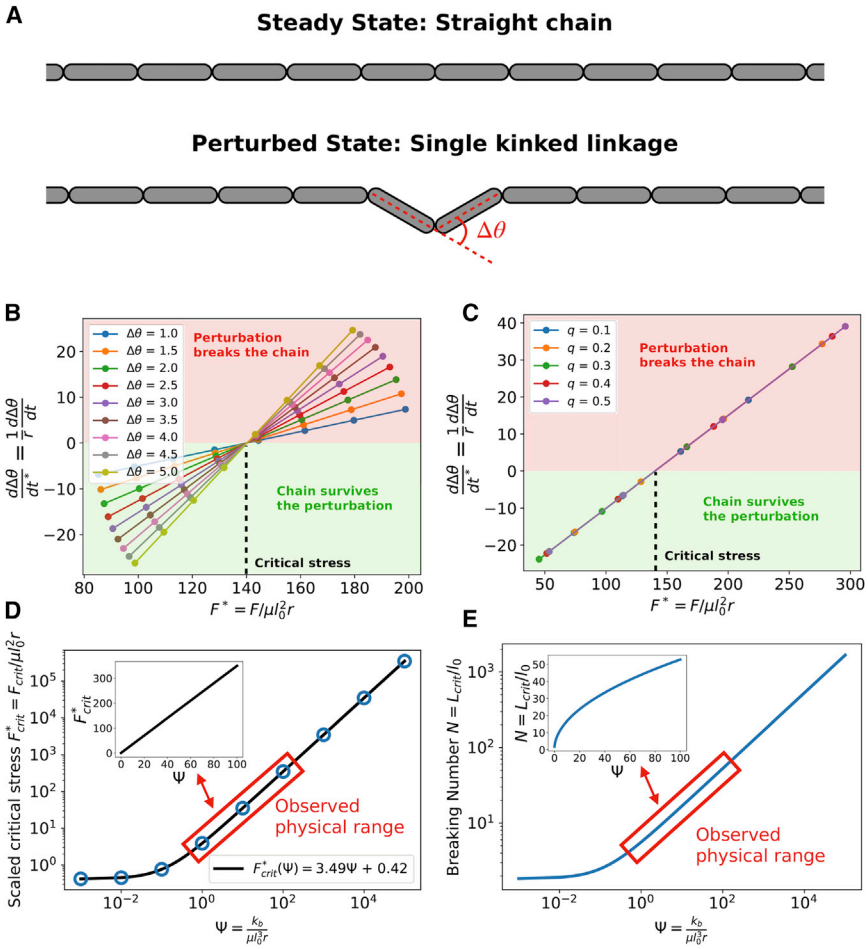

FIGURE 3 Perturbation analysis provides an estimate of the critical breaking stress as a function of the physical parameters. (*A*) Definition of the system's states used in the perturbation analysis. The steady state in our perturbation theory is a perfectly straight chain (*top*). The perturbed state deviates from the perfectly straight steady state only in one kinked cell-cell linkage (*bottom*). $\Delta\theta$ is used to define the size of the perturbation. $\Delta\dot{\theta} > 0$ corresponds to the system moving away from the perfectly straight steady state, while $\Delta\dot{\theta} < 0$ corresponds to the system moving toward the steady state. (*B* and *C*) The horizontal stress in a perfectly straight chain at the to-be-perturbed linkage is plotted against the instantaneous rate of change of the angle upon perturbation for various perturbations sizes (*B*) and various perturbation locations in the chain (*C*). The stress in the linkage is varied by varying the length of the chain. $\Delta\dot{\theta}$ transitions from a negative value to a positive value as the stress increases past a critical stress that is identical for all perturbation sizes (*B*) and all perturbation locations (*C*). The computations for (*B*) and (*C*) used $\Psi = 40$. The nondimensional parameter Ψ is defined by Eq. 1. (*D*) The computed critical stresses as a function of Ψ. The critical stress depends linearly on Ψ. The black line shows the linear function fitted to the computed data. (*E*) The critical breaking number (of cells in the chain), i.e., the nondimensionalized chain length at which breaks occur, varies as a function of the nondimensional parameter Ψ. In *C. perfringens*, breaks are typically observed to occur for chains with 10–50 cells (Fig. S3), suggesting that the physical range of Ψ for *C. perfringens* is $1 < \Psi < 100$. The same range is marked on (*D*), and zoom ins of the plots in this range are shown in the insets of (*D*) and (*E*). To see this figure in color, go online.

in a chain. Recall that the stress is highest at the center of the chain and decreases toward the tip of the chain (Eq. 2; Fig. 2 *B*). When $\Delta\dot{\theta}$ is computed for chains of different lengths perturbed at different relative locations (different q values), the stress-versus-$\Delta\dot{\theta}$ curves for different locations perfectly overlap (Fig. 3 *C*). This result and those above confirm that the instantaneous horizontal stress at a given linkage in a perfectly straight chain is sufficient to determine whether the chain will break immediately when perturbed at the linkage.

The critical stress that causes the chain to break depends on the physical parameters that govern the dynamics of the system. Most key physical parameters of the system are coupled through the nondimensional parameter $\Psi = k_b/\mu l_0^3 r$, which was revealed through nondimensionalization of the rigid rod equations (supporting material, Section S2.2) and relates the angular spring constant k_b, parallel drag coefficient per unit length μ, daughter cell length l_0, and growth rate r. We computed the critical stress associated with various values of Ψ using the process outlined above (method described in supporting material, Section S3) and found a linear relationship between the critical stress and Ψ (Fig. 3 *D*). Performing a linear fit on the data provided the nondimensionalized critical stress as a function of Ψ: $F^*_{crit} = m\,\Psi + z$, with $m = 3.49$ and $z = 0.42$. Additionally, longer chains experience larger stresses, and hence a larger critical stress value corresponds to a longer breaking length for a chain. Note that the nondimensionalized critical stress and nondimensionalized breaking length are related by $L_{crit}/l_0 = \left(8F_{crit}/\mu r l_0^2\right)^{1/2}$ (from Eq. 2 with $t = 0$ and $L_{crit} = N_{crit} l_0$). Hence, the nondimensionalized breaking length scales roughly with $\Psi^{1/2}$ (Fig. 3 *E*, *inset*). In *C. perfringens*, experimental observations suggest that chains typically break when the number of cells in the chains falls in the range $10 \lesssim N \lesssim 50$ (Fig. S3). This predicts a range of Ψ values for *C. perfringens* chains to be $1 \leq \Psi \leq 100$ (Fig. 3 *D*, *E*, *red boxes* and *insets*). Overall, the critical stress and typical breaking length of the cell chain both increase as the nondimensional parameter Ψ increases.

The critical stress and breaking length also depend on two additional coefficients a and b (supporting material, Section S3), which relate the perpendicular and rotational drag coefficients to the parallel drag coefficient. However, variation in these parameters results in only a small variation in the predicted critical stress and breaking length (Fig. S4). These small variations and the fact that a and b are physically restricted to a small range of values make the dependence of the critical stress and breaking length on a and b negligible.

Next, we re-dimensionalized the predicted linear relationship between the nondimensionalized critical stress and Ψ and obtained the relationship between the critical stress and all of the key physical parameters:

$$F_{crit} = m\frac{k_b}{l_0} + z\mu r l_0^2. \tag{3}$$

Furthermore, setting the dimensional critical stress equal to Eq. 2 from the rigid-rod model, we can determine the critical breaking length as a function of all of the key physical parameters:

$$L_{crit} = \left[8\left(m\frac{k_b}{\mu r l_0} + z l_0^2\right)\right]^{1/2}. \tag{4}$$

Equations 3 and 4 provide insights to how the critical stress and breaking length scale with each physical parameter. First, and most interestingly, the critical stress and breaking length depend on l_0 in a biphasic manner (Fig. 4 *A*). This is because the critical stress and breaking length are contributed by two terms with opposite dependence on l_0 (Eqs. 3 and 4). With strong cell-cell linkages (large k_b) or low drag (small μ), mechanical integrity of the chain is strengthened by smaller cell lengths, and vice versa with weak cell-cell linkages (small k_b) or high drag (large μ). Second, the critical stress increases, while the breaking length decreases, with increasing cell growth rate r (Fig. 4 *B*). These opposite trends can be understood as faster cell growth results in higher cell velocities at the same chain length and requires larger stresses to propel

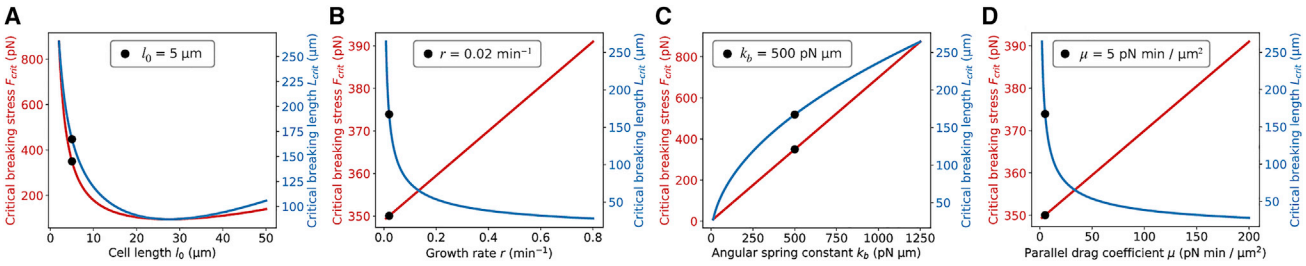

FIGURE 4 Predicted critical breaking stress F_{crit} and length L_{crit} as functions of each physical parameter. (*A*) The breaking stress and breaking length vary in a biphasic manner with respect to the cell length l_0. (*B*) The breaking stress increases as the growth rate r increases, while the breaking length decreases. (*C*) The breaking stress and length increase as the angular spring constant k_b increases. (*D*) The breaking stress increases for substrates with a larger parallel drag coefficient per unit length μ, while the breaking length decreases. All plots generated according to Eq. 4. The following default parameter values are used whenever a parameter is held fixed: $l_0 = 5$ μm, $r = 0.02$ min^{-1}, $k_b = 500$ pN μm, $\mu = 5$ pN min/μm^2, $m = 3.49$, and $z = 0.42$. The default parameter values are denoted with black dots in each plot and correspond to $\Psi = 40$. The range for l_0 in (*A*) was chosen to display the biphasic nature of the relation for this parameter. (*B*)–(*D*) span the range of $1 < \Psi < 100$. To see this figure in color, go online.

the cells. In the end, although the critical stress increases with faster growth rate r, it will be reached at a shorter chain length. Third, the critical stress and breaking length both increase with the angular spring constant k_b for the cell-cell linkages (Fig. 4 *C*). This means that more rigid cell-cell linkages can withstand larger forces and allow the chains to grow to longer lengths. Lastly, the critical stress and breaking length depend on the drag coefficient μ similar to their dependence on the cell growth rate r (Fig. 4 *D*). Evidently, higher drag from the substrate would increase the stress in the linkages between adjacent cells. Like above, although the critical stress increases with higher drag, it is reached at a shorter chain length. In summary, understanding how the critical breaking stress depends on the physical parameters provides quantitative insights to the mechanical limitation of cell-chain-mediated motility and provides experimentally testable predictions.

Breaks limit the long-term expansion rate of bacterial chains

In the previous section, we showed that bacterial chains tend to break if the stress at a cell-cell linkage exceeds a critical level. Since the total growth rate of the bacterial chain is given by $L'(t) = Nl_0re^{rt} = L(t)r$, shorter chains grow slower than longer chains. Hence, chain breakage will reduce the expansion of the bacterial population into the surrounding environment. To evaluate the effect of chain breakage on the expansion of the bacterial population, we developed a simplistic phenomenological model (Fig. 5 *A*) that tracks the expansion and breakage of chains over time, based on the critical breaking stress predicted in the previous section. We then used the model to estimate the effective expansion rate of the bacterial population driven by the cell-chain-mediated mechanism.

The phenomenological population-expansion model aims at a rough estimation of the chain expansion rate and only considers expansion in one dimension. Particularly, the model assumes that all the chains are perfectly straight and that after a chain breaks, the resulting two chains remain parallel and continue to expand from their respective free tips (Fig. 5 *A*). Such an assumption was motivated by the experimental observation that after a *C. perfringens* chain breaks, the two new chains usually maintain lateral adherence to each other during their following expansion (Video S9). In the model, the chain is initialized with a small number of cells with the typical length of a daughter cell l_0. The individual cells in the chain grow exponentially and divide simultaneously. Over time, the chain grows longer and expands outward, while the stress in each cell-cell linkage rises. Once the stress in a linkage exceeds the critical stress $F^*_{crit}(\Psi)$ predicted by the rigid-rod model above, the chain will break at the linkage and divide into two shorter chains, each expanding in both directions (Fig. 5 *A*). Overlap between the two new chains reduces the overall efficiency of expansion of the bacterial population, since multiple cells are now exploring the same region. Over long periods of time, this pattern repeats itself. Eventually, the system comes to consist of numerous overlapping chains expanding into their surroundings.

The model tracks the expansion distance of the bacterial population, which is defined as the distance from the leftmost chain tip to the rightmost chain tip (Fig. 5 *A*). Let us first consider the noise-less case, in which all the cell-cell linkages are equally strong, and the cell cycles are perfectly synchronized. In this case, the break always occurs in the center linkage at the predicted critical breaking length; the two new chains will each have a length equal to half of the critical breaking length. Consequently, as the population grows, the expansion distance increases exponentially until the first break occurs (Fig. 5 *B*). The break induces an abrupt drop in the expansion rate (Fig. 5 *C*). Following the break, the population is able to regain exponential expansion, but the next chain break will again cut the expansion rate of the population (Fig. 5 *C*). Over multiple cell cycles, these periods of exponential growth followed by breakages average out to a constant rate of expansion (Fig. 5 *B* and *C*). Therefore, these results reveal a maximum population expansion rate constrained by the mechanical limitation of single-chain growth. We also considered simulations with stochastic effects (supporting material, Section S4), including asynchronous cell division and mechanical variations in the cell-cell linkages, but these effects did not change the expansion rates significantly (Fig. S5).

The noise-less case further allows us to analytically derive the expansion rate and determine its dependence on the fundamental parameters in the system. In the noise-less case, once a chain breaks in half, it will take exactly one doubling time for the two smaller chains to each grow to the critical breaking length. Therefore, breakage events will always be separated by the doubling time $\tau = ln2/r$. Additionally, during each of these intervals, the leftmost and rightmost chains in the population will always expand further out by a distance of one-fourth the critical breaking length, which sum up to an overall population expansion of half the critical breaking length. From these values, we find the expected relationship between the final average expansion rate and the critical breaking length to be $\dot{D} = r\,L_{crit} \,/\, 2\ln 2$. Rearranged to the nondimensionalized form, the relationship reads

$$\frac{\dot{D}}{l_0 r} = \frac{L_{crit}/l_0}{2\ln 2}. \tag{5}$$

According to Eq. 5, the scaled expansion rate $\frac{\dot{D}}{l_0 r}$ and the breaking number L_{crit}/l_0 should differ by only a constant value. Plotting the scaled expansion rates from the simulation against the critical breaking numbers indeed gives a linear relationship between the two values with a slope of $(2\ln 2)^{-1}$, as predicted by Eq. 5 (Fig. 5 *D*). Recall that the

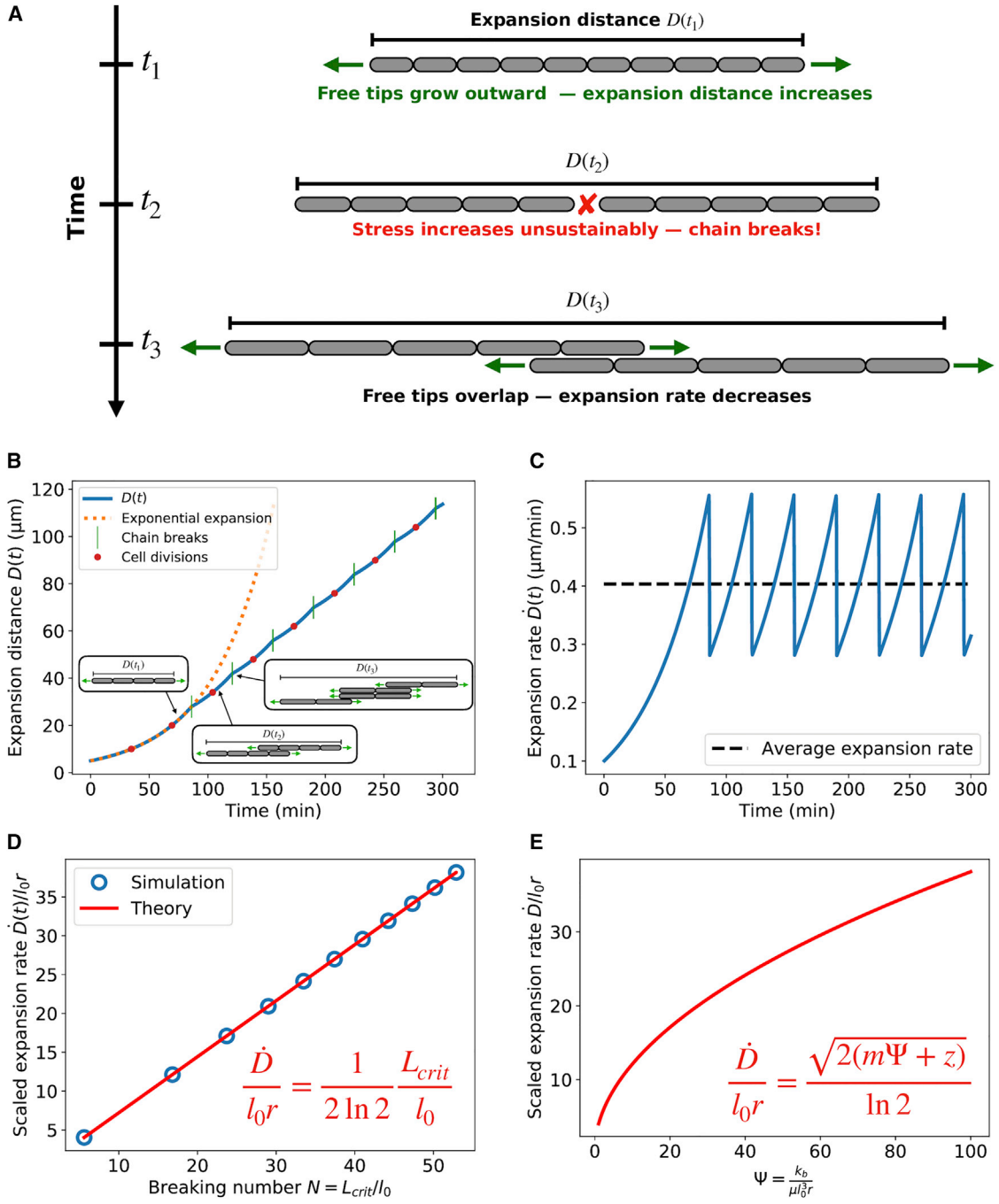

FIGURE 5 Population-expansion model predicts expansion dynamics of a bacterial chain population. (*A*) Model setup. The initial chain grows with two free ends expanding outward. Once the chain grows long enough, the stress in one of the linkages of the chain will exceed the critical breaking stress predicted by the rigid-rod model. The chain will then break into two shorter chains, each with two free ends. The two separate chains both freely expand outward but overlap with one another in the process. The overlap slows down the overall expansion of the bacterial population. (*B*) The expansion distance of the population as a function of time for a single run of the model with $\Psi = 1$ in the noise-less case (i.e., perfectly synchronized cell cycle and identical strength of cell-cell linkages). $\Psi = 1$ was chosen because the corresponding breaking length is small, making it easy to illustrate the expansion dynamics. Cell division occurs at a fixed interval determined by the growth rate of the cells. The gray boxes depict configurations of the chains in the system at three different time points. It should be noted that while it appears that chain breaks always occur right in the middle between division events, this is only a coincidence: chain breaks can occur at any point in the cell cycle depending on the particular parameter set and initial conditions. (*C*) The expansion rate of the population as a function of time for a single run of the model with $\Psi = 1$ in the noise-less case. The expansion rate increases exponentially between breaks. The breakages cause a drop in the expansion rate (exactly half after the first break). Over long periods of time, this pattern averages out to a constant expansion rate (*dotted black line*). (*D*) The scaled expansion rate is proportional to the critical breaking number. This relationship is predicted analytically (*red line*) and numerically through simulation (*blue circles*). (*E*) Analytically derived expansion rate as a function of Ψ. To see this figure in color, go online.

perturbation analysis of the rigid-rod model predicted the critical breaking length as a function of Ψ : $L_{crit} = 2l_0\sqrt{2(m\Psi + z)}$. Combining this equation with Eq. 5 yields a theoretical expression for the expansion rate as a function of Ψ (Fig. 5 *E*):

$$\frac{\dot{D}}{l_0 r} = \frac{[2(m\Psi + z)]^{1/2}}{\ln 2}. \quad (6)$$

The scaled expansion rate increases as Ψ increases, but the curve flattens for larger values, indicating a diminishing return in the expansion efficiency for larger values of Ψ.

Remembering $\Psi = k_b/\mu l_0^3 r$, we rearrange Eq. 6 to determine how the population expansion rate depends on each physical parameter:

$$\dot{D} = \frac{1}{\ln 2}\left\{2\left[m\left(\frac{k_b r}{\mu l_0}\right) + z r^2 l_0^2\right]\right\}^{1/2}. \quad (7)$$

The relationships between the expansion rate and the physical parameters are summarized in Fig. 6. Most of these relationships are similar to the predicted dependence of the breaking number on the physical parameters (Fig. 4), including a biphasic dependence on the cell length l_0 (Fig. 6 *A*), a positive dependence on the angular spring constant k_b (Fig. 6 *C*), and a negative dependence on the drag coefficient μ (Fig. 6 *D*). Only the dependence on the cell-growth rate r has turned positive in the expansion rate (Fig. 6 *B*). These relationships suggest potential mechanisms that bacteria may adopt to enhance long-term population expansion driven by the cell-chain-mediated motility. For example, stronger cell-cell linkage would apparently promote the population expansion rate. Additionally, these predicted relationships can be experimentally tested through mutant strains or varied experimental conditions.

DISCUSSION

In this work, we found that cell-chain-mediated bacterial sliding motility is likely widespread in gram-positive bacteria and developed a novel physics-based mechanical model (the rigid-rod model) to analyze its mechanical limitation. The model depicts the fundamental processes governing the chain growth, including cell growth, cell division, cell-cell connection, and cell-substrate interaction. The model shows an exponential increase in the stress at the linkages between adjacent cells as the number of cells in the chain grows exponentially. Such an exponential increase in stress is unsustainable over long periods of time. Perturbation analysis of the rigid-rod model reveals the critical stress and critical breaking length, upon which the chain would break after small perturbations, most likely at the center linkage that sustains the highest stress. We further developed a phenomenological population-expansion model that uses the findings from the rigid-rod model to make computationally efficient estimations of the chain-mediated expansion of a bacterial population over a long period of time. The model shows that chain breakages prevent exponential expansion of the bacterial population and set an upper bound on the expansion rate.

Importantly, our models provide several testable predictions for the expansion dynamics of bacterial chains. The perturbation analysis of the rigid-rod model predicts the dependence of the critical breaking stress and length of the chains on each of the key physical parameters (Fig. 4). This analysis shows that the critical breaking stress is most sensitive to variations in the cell length and angular spring constant and less sensitive to the cell-growth rate and drag coefficient. Interestingly, both the breaking stress and the breaking length exhibit a biphasic dependence on the cell length. These biphasic relations reveal a characteristic cell length that minimizes the breaking stress and length, though the biological significance of such a minimum is unclear. The population-expansion model further provides testable predictions for the estimated expansion rate of the bacterial chain population as a function of the physical parameters (Fig. 6). The estimated expansion rate is sensitive to all four of the physical parameters and is most sensitive to variations in the cell-growth rate. The expansion rate depends on the cell length in a biphasic

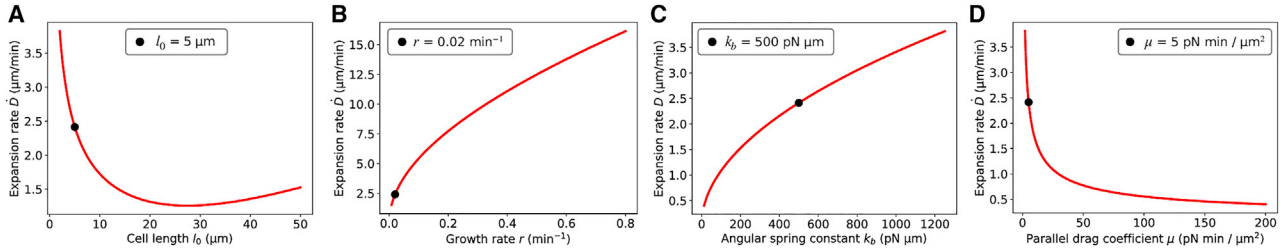

FIGURE 6 Predicted population expansion rate as a function of each physical parameter. (*A*) The expansion rate varies with respect to the cell length l_0 in a biphasic manner. (*B*) The expansion rate increases as the growth rate r increases. (*C*) The expansion rate increases as the angular spring constant k_b increases. (*D*) The expansion rate decreases as the parallel drag coefficient per unit length μ increases. All plots were generated according to Eq. 6. The following default parameter values are used whenever a parameter is held fixed: $l_0 = 5$ μm, $r = 0.02$ min^{-1}, $k_b = 500$ pN μm, $\mu = 5$ pN min/μm^2, $m = 3.49$, and $z = 0.42$. The default parameter values are denoted with black dots in each plot and correspond to $\Psi = 40$. The range for l_0 in (*A*) was chosen to display the biphasic nature of the relation for this parameter. (*B*)–(*D*) span the range of $1 < \Psi < 100$. To see this figure in color, go online.

manner similar to the critical breaking stress and length. Note that since only expansion in one dimension is considered, the population-expansion model likely overestimates the expansion rate—expansion in other dimensions in reality would slow down the expansion but allow the bacterial population to navigate larger space. Given the simplifications taken in the population-expansion model, its predictions should be viewed in a more qualitative manner rather than taken as a definitive quantification.

The model predictions suggest possible ways the bacteria could evolve to enhance the cell-chain-mediated motility and achieve a longer breaking length and/or higher colony expansion rate. Based on the predictions given in Fig. 4, the most efficient ways to delay chain breaks include avoiding overly long cells and increasing the mechanical strength of the cell-cell linkages. Interestingly, the latter strategy might have been exploited by *C. perfringens*, *B. megaterium*, and *B. subtilis* through lateral support between neighboring cell chains. Although our model focuses on the dynamics of a single, isolated chain, experimental observations show that chains of the above bacteria often grow in parallel rather than in isolation (Video S10), which likely evolves from the frequently observed lateral adherence between segments of newly broken chains over many cycles of breakages (Videos S2, S3, S4, and S11). Such multi-chains are likely more resistant to bending, as the chains are laterally fortified by their neighbors. According to our model results, increasing the angular spring constant of cell-cell linkages would increase the critical breaking stress and breaking length (Fig. 4 *C*) and foster faster population expansion (Fig. 6 *C*). With lateral fortification, the chain is expected to be less prone to bending, corresponding to an effective increase in the spring constant of the cell-cell linkages. Applying concepts from solid mechanics, we can perform a back-of-the-envelope estimate of the bending rigidity of a multi-chain. In the worst-case scenario, parallel chains freely slide relative to their neighbors without any friction. In this situation, the bending rigidity of the multi-chain, which roughly corresponds to the effective angular spring constant k_b^{eff}, would scale linearly with the number of chains in parallel. In the best-case scenario, the parallel chains would not slip relative to each other at all, essentially forming one solid structure. In this scenario, the bending rigidity would scale with the number of chains in parallel cubed (61). Taken together, in a situation with M chains growing in parallel, the effective angular spring constant would scale with the number of chains between $k_b^{eff} = M$ and $k_b^{eff} = M^3$. Based on the results of the expansion model, the expansion rate scales as $\dot{D} = k_b^{1/2}$. Hence, the expansion rate of M chains growing in parallel would scale between $\dot{D} = M^{1/2}$ and $\dot{D} = M^{3/2}$. Our future investigations will detail the effects of multiple chains growing together and quantify any advantages multi-chains may have as a mechanism for bacterial population expansion.

The mechanical rigid-rod model provides a powerful theoretical and computational framework for studying the cell-chain-mediated bacterial motility. Compared with previous models developed for the chain dynamics in *B. subtilis* (52,53), our model provides the equations of motion for each individual cell as the chain grows. These equations of motion not only allow more efficient and stable simulations for long-term chain dynamics than the classical mass-spring models for moving rod-shaped bacteria (62,63) but also provide a convenient framework for mechanical-instability analysis (i.e., our analysis for the critical breaking stress). Most strikingly, with the convenient assumption of synchronous exponential growth, which does not affect the conclusion, the nondimensionalized model practically depends on only one free parameter, Ψ. This eliminates the problem of parameter uncertainty, an issue that pesters many biological models, and allows us to make highly reliable predictions on the relationship between the critical breaking stress/length and the model parameters. Furthermore, formulating the equations using Lagrangian mechanics allows for straightforward quantification of the stress in each cell-cell linkage: the x and y components of the stress are identical to the Lagrange multipliers in the constraint conditions that represent the connections between adjacent cells. This forgoes an explicit account of the unknown expansive force for cell growth and cell division. Finally, the use of Lagrangian mechanics allows the rigid-rod model to easily include additional conservative or constraint forces in the future, e.g., in the study of chain-chain interactions.

Note that the perturbation analysis used to quantify the critical breaking stress is similar to the linear stability analysis for dynamical systems. While the system we present here is continuously growing and lacks a true steady state, the concepts are still applicable. In this analysis, a perfectly straight chain was considered to be the steady state of the system, since a chain with a perfectly straight initial condition will always remain perfectly straight as it grows. We then considered a slightly kinked state as the small perturbation in the linear stability analysis. A kinked chain will experience one of two possible outcomes: 1) the steady state is stable: the system will move toward the steady state, i.e., the kink flattens, or 2) the steady state is unstable: the system will move away from the steady state, i.e., the kink exacerbates, leading to chain breakage. The point at which the system transitions between these two cases defines the critical stress of the system, similar to how the change of sign in the Jacobian of an ordinary differential equation system marks the bifurcation point where the steady state changes from stable to unstable.

A number of our conclusions are consistent with the few previous models for expanding bacterial chains developed with different methods. For example, the parabolic stress profile in Eq. 2. agrees with previous derivations in the continuum limit (53,64). In addition, the biphasic dependence of the critical breaking stress and breaking length on the

cell length and the decrease of critical breaking length with increasing cell-substrate drag coefficient predicted by our model are similar to those predicted by a previous chain-dynamics model that also resolves single cells (53). Because the model in (53) involves different assumptions about the cell-substrate interaction and assumes elastic interactions between adjacent cells (unlike our model with hard constraints between adjacent cells), the predictions from the two models bear quantitative differences.

It is interesting to compare the role of mechanical instabilities in chain expansion versus in 2D biofilm expansion. Mechanical instability in 2D biofilms leads to verticalization (28–30), wrinkling (31–33), and 2D-to-3D transitions (29,34,35). In other words, mechanical instability in the 2D biofilm gives rise to dynamics in the new vertical dimension. But in most cases, the growth of the biofilm in the vertical direction is small compared with the in-plane direction, and hence the biofilm will not compromise significantly in its outward expansion. This is also true in chain expansion: breaking of the chain leads to development of multi-chains, as mentioned above. However, these multi-chain structures tend to largely continue with directed one-dimensional expansion, as the single chains are aligned in these structures. As such, while the mechanical failure of cell-cell linkages may limit the efficacy of the chain-mediated sliding motility, the one-dimensional tendency of the expansion persists, which helps the bacteria spread faster over distances.

Overall, our work highlights mechanical limitation as an important consideration in cell-chain-mediated motility and creates an extensible framework for future study of such motility. This motility mechanism not only offers potential advantages in speed and energy efficiency but may also be more widespread in bacteria than currently known, as it can be enabled by a few genetic or phenotypic changes that inhibit the final septation step of bacterial division. As strong cell-cell connections are critical for effective cell-chain-mediated motility, gram-positive bacteria may be more likely to acquire this motility, as their thick peptidoglycan provides a stiff material to form strong cell-cell linkages. Taken together, studying this motility mechanism will likely open up new opportunities to control pathogenicity and other phenotypes of gram-positive bacteria.

SUPPORTING MATERIAL

Supporting material can be found online at https://doi.org/10.1016/j.bpj.2022.05.012.

AUTHOR CONTRIBUTIONS

J.C. and S.B.M. designed research; S.G.M. and J.C. developed mathematical models and performed model analyses; S.G.M. performed model simulations; S.B.M. performed experiments; S.G.M. and S.B.M. processed experimental movies and analyzed data; and S.G.M., S.B.M., and J.C. wrote the manuscript.

ACKNOWLEDGMENTS

We thank Prof. John C. Neu for valuable discussions and Donna Melville for technical assistance with movies. This work was supported by NIH grants 1R35GM138370 (J.C.), 1R21AI109391 (S.B.M.), and 1R21AI149177 (S.B.M.).

DECLARATION OF INTERESTS

The authors declare no competing interests.

SUPPORTING CITATIONS

References (65-67) appear in the supporting material.

REFERENCES

1. Jarrell, K. F., and M. J. McBride. 2008. The surprisingly diverse ways that prokaryotes move. *Nat. Rev. Microbiol.* 6:466–476. https://doi.org/10.1038/nrmicro1900.
2. McBride, M. J. 2001. Bacterial gliding motility: multiple mechanisms for cell movement over surfaces. *Annu. Rev. Microbiol.* 55:49–75. https://doi.org/10.1146/annurev.micro.55.1.49.
3. Wadhwa, N., and H. C. Berg. 2021. Bacterial motility: machinery and mechanisms. *Nat. Rev. Microbiol.* 20:161–173. https://doi.org/10.1038/s41579-021-00626-4.
4. Miyata, M., R. C. Robinson, …, K. I. Wakabayashi. 2020. Tree of motility - a proposed history of motility systems in the tree of life. *Gene Cell.* 25:6–21. https://doi.org/10.1111/gtc.12737.
5. Berg, H. C. 2003. The rotary motor of bacterial flagella. *Annu. Rev. Biochem.* 72:19–54. https://doi.org/10.1146/annurev.biochem.72.121801.161737.
6. Nakamura, S., and T. Minamino. 2019. Flagella-driven motility of bacteria. *Biomolecules.* 9:279. https://doi.org/10.3390/biom9070279.
7. Berg, H. C., and R. A. Anderson. 1973. Bacteria swim by rotating their flagellar filaments. *Nature.* 245:380–382. https://doi.org/10.1038/245380a0.
8. Burrows, L. L. 2005. Weapons of mass retraction. *Mol. Microbiol.* 57:878–888. https://doi.org/10.1111/j.1365-2958.2005.04703.x.
9. Nudleman, E., and D. Kaiser. 2004. Pulling together with type IV pili. *J. Mol. Microbiol. Biotechnol.* 7:52–62. https://doi.org/10.1159/000077869.
10. Mattick, J. S. 2002. Type IV pili and twitching motility. *Annu. Rev. Microbiol.* 56:289–314. https://doi.org/10.1146/annurev.micro.56.012302.160938.
11. Melville, S., and L. Craig. 2013. Type IV pili in Gram-positive bacteria. Microbiology and molecular biology reviews. *Microbiol. Mol. Biol. Rev.* 77:323–341. https://doi.org/10.1128/MMBR.00063-12.
12. Pelicic, V. 2019. Monoderm bacteria: the new frontier for type IV pilus biology. *Mol. Microbiol.* 112:1674–1683. https://doi.org/10.1111/mmi.14397.
13. Kobayashi, K., N. Kodera, …, M. Miyata. 2021. Movements of mycoplasma mobile gliding machinery detected by high-speed atomic force microscopy. *mBio.* 12:e0004021. https://doi.org/10.1128/mBio.00040-21.
14. Miyata, M., and T. Hamaguchi. 2016. Prospects for the gliding mechanism of Mycoplasma mobile. *Curr. Opin. Microbiol.* 29:15–21. https://doi.org/10.1016/j.mib.2015.08.010.
15. Chen, J., J. Neu, …, G. Oster. 2009. Motor-substrate interactions in mycoplasma motility explains non-Arrhenius temperature dependence. *Biophys. J.* 97:2930–2938. https://doi.org/10.1016/j.bpj.2009.09.020.
16. Miyata, M., W. S. Ryu, and H. C. Berg. 2002. Force and velocity of mycoplasma mobile gliding. *J. Bacteriol.* 184:1827–1831.

17. Jaffe, J. D., M. Miyata, and H. C. Berg. 2004. Energetics of gliding motility in Mycoplasma mobile. *J. Bacteriol.* 186:4254–4261. https://doi.org/10.1128/JB.186.13.4254-4261.2004.

18. Nan, B. 2017. Bacterial gliding motility: rolling out a consensus model. *Curr. Biol.* 27:R154–R156. https://doi.org/10.1016/j.cub.2016.12.035.

19. Nan, B., M. McBride, …, G. Oster. 2014. Bacteria that glide with helical tracks. *Curr. Biol.* 24:R169–R173. https://doi.org/10.1016/j.cub.2013.12.034.

20. Nan, B., J. Chen, …, D. R. Zusman. 2011. Myxobacteria gliding motility requires cytoskeleton rotation powered by proton motive force. *Proc. Natl. Acad. Sci. U. S. A.* 108:2498–2503. https://doi.org/10.1073/pnas.1018556108.

21. Faure, L. M., J. B. Fiche, …, T. Mignot. 2016. The mechanism of force transmission at bacterial focal adhesion complexes. *Nature.* 539:530–535. https://doi.org/10.1038/nature20121.

22. Shaevitz, J. W., J. Y. Lee, and D. A. Fletcher. 2005. Spiroplasma swim by a processive change in body helicity. *Cell.* 122:941–945. https://doi.org/10.1016/j.cell.2005.07.004.

23. Wada, H., and R. R. Netz. 2009. Hydrodynamics of helical-shaped bacterial motility. *Phys. Rev.* 80:021921. https://doi.org/10.1103/PhysRevE.80.021921.

24. Sasajima, Y., and M. Miyata. 2021. Prospects for the mechanism of Spiroplasma swimming. *Front. Microbiol.* 12:706426. https://doi.org/10.3389/fmicb.2021.706426.

25. Holscher, T., and A. T. Kovacs. 2017. Sliding on the surface: bacterial spreading without an active motor. *Environ. Microbiol.* 19:2537–2545. https://doi.org/10.1111/1462-2920.13741.

26. Henrichsen, J. 1972. Bacterial surface translocation: a survey and a classification. *Bacteriol. Rev.* 36:478–503. https://doi.org/10.1128/br.36.4.478-503.1972.

27. Harshey, R. M. 2003. Bacterial motility on a surface: many ways to a common goal. *Annu. Rev. Microbiol.* 57:249–273. https://doi.org/10.1146/annurev.micro.57.030502.091014.

28. Beroz, F., J. Yan, …, Y. Meir. 2018. Verticalization of bacterial biofilms. *Nat. Phys.* 14:954–960. https://doi.org/10.1038/s41567-018-0170-4.

29. Drescher, K., J. Dunkel, …, B. L. Bassler. 2016. Architectural transitions in Vibrio cholerae biofilms at single-cell resolution. *Proc. Natl. Acad. Sci. U. S. A.* 113:E2066–E2072. https://doi.org/10.1073/pnas.1601702113.

30. Hartmann, R., P. K. Singh, …, K. Drescher. 2019. Emergence of three-dimensional order and structure in growing biofilms. *Nat. Phys.* 15:251–256. https://doi.org/10.1038/s41567-018-0356-9.

31. Fei, C., S. Mao, …, A. Kosmrlj. 2020. Nonuniform growth and surface friction determine bacterial biofilm morphology on soft substrates. *Proc. Natl. Acad. Sci. U. S. A.* 117:7622–7632. https://doi.org/10.1073/pnas.1919607117.

32. Yan, J., C. Fei, …, B. L. Bassler. 2019. Mechanical instability and interfacial energy drive biofilm morphogenesis. *Elife.* 8:e43920. https://doi.org/10.7554/eLife.43920.

33. Zhang, C., B. Li, …, X. Q. Feng. 2017. Experimental and theoretical studies on the morphogenesis of bacterial biofilms. *Soft Matter.* 13:7389–7397. https://doi.org/10.1039/c7sm01593c.

34. Warren, M. R., H. Sun, …, T. Hwa. 2019. Spatiotemporal establishment of dense bacterial colonies growing on hard agar. *Elife.* 8:e41093. https://doi.org/10.7554/eLife.41093.

35. You, Z., D. J. Pearce, …, L. Giomi. 2019. Mono- to multilayer transition in growing bacterial colonies. *Phys. Rev. Lett.* 123:178001. https://doi.org/10.1103/PhysRevLett.123.178001.

36. Dervaux, J., J. C. Magniez, and A. Libchaber. 2014. On growth and form of Bacillus subtilis biofilms. *Interface Focus.* 4:20130051. https://doi.org/10.1098/rsfs.2013.0051.

37. Pearce, P., B. Song, …, J. Dunkel. 2019. Flow-induced symmetry breaking in growing bacterial biofilms. *Phys. Rev. Lett.* 123:258101. https://doi.org/10.1103/PhysRevLett.123.258101.

38. Doumic, M., S. Hecht, and D. Peurichard. 2020. A purely mechanical model with asymmetric features for early morphogenesis of rod-shaped bacteria micro-colony. *Math. Biosci. Eng.* 17:6873–6908. https://doi.org/10.3934/mbe.2020356.

39. Nijjer, J., C. Li, …, J. Yan. 2021. Mechanical forces drive a reorientation cascade leading to biofilm self-patterning. *Nat. Commun.* 12:6632. https://doi.org/10.1038/s41467-021-26869-6.

40. Qin, B., C. Fei, …, B. L. Bassler. 2021. Hierarchical transitions and fractal wrinkling drive bacterial pellicle morphogenesis. *Proc. Natl. Acad. Sci. U. S. A.* 118. https://doi.org/10.1073/pnas.2023504118.

41. Zhang, Q., J. Li, …, J. Yan. 2021. Morphogenesis and cell ordering in confined bacterial biofilms. *Proc. Natl. Acad. Sci. U S A.* 118. https://doi.org/10.1073/pnas.2107107118.

42. Liu, H., L. Bouillaut, …, S. B. Melville. 2013. Use of a mariner-based transposon mutagenesis system to isolate Clostridium perfringens mutants deficient in gliding motility. *J. Bacteriol.* 195:629–636. https://doi.org/10.1128/JB.01288-12.

43. Liu, H., K. D. McCord, …, S. B. Melville. 2014. Hypermotility in Clostridium perfringens strain SM101 is due to spontaneous mutations in genes linked to cell division. *J. Bacteriol.* 196:2405–2412. https://doi.org/10.1128/JB.01614-14.

44. Varga, J. J., V. Nguyen, …, S. B. Melville. 2006. Type IV pili-dependent gliding motility in the Gram-positive pathogen Clostridium perfringens and other Clostridia. *Mol. Microbiol.* 62:680–694. https://doi.org/10.1111/j.1365-2958.2006.05414.x.

45. Varga, J. J., B. Therit, and S. B. Melville. 2008. Type IV pili and the CcpA protein are needed for maximal biofilm formation by the gram-positive anaerobic pathogen Clostridium perfringens. *Infect. Immun.* 76:4944–4951. https://doi.org/10.1128/IAI.00692-08.

46. Mendez, M., I. H. Huang, …, M. R. Sarker. 2008. Carbon catabolite repression of type IV pilus-dependent gliding motility in the anaerobic pathogen Clostridium perfringens. *J. Bacteriol.* 190:48–60. https://doi.org/10.1128/JB.01407-07.

47. Stevens, D. L. 1997. Necrotizing Clostridial soft tissue infections. *In* The Clostridia: Molecular Biology and Pathogenesis. J. I. Rood, B. A. McClane, J. G. Songer, and R. W. Titball, eds Academic Press, San Diego, CA, pp. 141–152.

48. Mendelson, N. H., J. J. Thwaites, …, C. Li. 1995. Mechanics of bacterial macrofiber initiation. *J. Bacteriol.* 177:7060–7069. https://doi.org/10.1128/jb.177.24.7060-7069.1995.

49. Klapper, I. 1996. Biological applications of the dynamics of twisted elastic rods. *J. Comput. Phys.* 125:325–337.

50. Wolgemuth, C. W., R. E. Goldstein, and T. R. Powers. 2004. Dynamic supercoiling bifurcations of growing elastic filaments. *Phys. Nonlinear Phenom.* 190:266–289. https://doi.org/10.1016/j.physd.2003.10.007.

51. Mamou, G., G. Malli Mohan, …, S. Ben-Yehuda. 2016. Early developmental program shapes colony morphology in bacteria. *Cell Rep.* 14:1850–1857. https://doi.org/10.1016/j.celrep.2016.01.071.

52. Yaman, Y. I., E. Demir, …, A. Kocabas. 2019. Emergence of active nematics in chaining bacterial biofilms. *Nat. Commun.* 10:2285. https://doi.org/10.1038/s41467-019-10311-z.

53. Liu, Y., B. Li, and X.-Q. Feng. 2020. Buckling of growing bacterial chains. *J. Mech. Phys. Solid.* 145:104146.

54. Goldstein, H. 1980. Classical Mechanics. Addison-Wesley.

55. Hinch, E. J. 1988. Hydrodynamics at low Reynolds numbers: a brief and elementary introduction. *In* Disorder and Mixing: Convection, Diffusion and Reaction in Random Materials and Processes. E. Guyon, J.-P. Nadal, and Y. Pomeau, eds Springer Netherlands, Dordrecht, pp. 43–56.

56. Trueba, F. J., and L. J. H. Koppes. 1998. Exponential growth of Escherichia coli B/r during its division cycle is demonstrated by the size distribution in liquid culture. *Arch. Microbiol.* 169:491–496. https://doi.org/10.1007/s002030050601.

57. Cooper, S. 2006. Distinguishing between linear and exponential cell growth during the division cycle: single-cell studies, cell-culture

studies, and the object of cell-cycle research. *Theor. Biol. Med. Model.* 3:10. https://doi.org/10.1186/1742-4682-3-10.

58. Cato, E. P., W. L. George, and S. M. Finegold. 1986. Genus Clostridium. *In* Bergey's Manual of Systematic Bacteriology. P. H. A. Sneath, N. S. Mair, M. E. Sharpe, and J. G. Holt, eds Williams & Wilkins, Baltimore, MD, pp. 1141–1200.

59. Shimizu, T., K. Ohtani, …, H. Hayashi. 2002. Complete genome sequence of Clostridium perfringens, an anaerobic flesh-eater. *Proc. Natl. Acad. Sci. U. S. A.* 99:996–1001. https://doi.org/10.1073/pnas.022493799.

60. Myers, G. S., D. A. Rasko, …, I. T. Paulsen. 2006. Skewed genomic variability in strains of the toxigenic bacterial pathogen, Clostridium perfringens. *Genome Res.* 16:1031–1040. https://doi.org/10.1101/gr.5238106.

61. Phillips, R., J. Kondev, and J. Theriot. 2008. Physical Biology of the Cell. Garland Science, Taylor & Francis Group, New York.

62. Balagam, R., D. B. Litwin, …, O. A. Igoshin. 2014. Myxococcus xanthus gliding motors are elastically coupled to the substrate as predicted by the focal adhesion model of gliding motility. *PLoS Comput. Biol.* 10:e1003619. https://doi.org/10.1371/journal.pcbi.1003619.

63. Janulevicius, A., M. C. van Loosdrecht, …, C. Picioreanu. 2010. Cell flexibility affects the alignment of model myxobacteria. *Biophys. J.* 99:3129–3138. https://doi.org/10.1016/j.bpj.2010.08.075.

64. Wolgemuth, C. 2000. Theory and Experiment on Thin Life at Low Reynolds Number. Department of Physics. The University of Arizona.

65. Hon, J. W., and M. A. L. R. Strutt. 1873. Some General Theorems Relating to Vibrations. London Mathematical Society.

66. Chen, K. C., A. Csikasz-Nagy, …, J. J. Tyson. 2000. Kinetic analysis of a molecular model of the budding yeast cell cycle. *Mol. Biol. Cell.* 11:369–391.

67. Kar, S., W. T. Baumann, …, J. J. Tyson. 2009. Exploring the roles of noise in the eukaryotic cell cycle. *Proc. Natl. Acad. Sci. U. S. A.* 106:6471–6476. https://doi.org/10.1073/pnas.0810034106.